atoms

MDPI

Article

Magnetic Sublevel Independent Magic and Tune-Out Wavelengths of the Alkaline-Earth Ions

Jyoti [1], Harpreet Kaur [1], Bindiya Arora [1,*] and Bijaya Kumar Sahoo [2]

[1] Department of Physics, Guru Nanak Dev University, Amritsar 143005, Punjab, India; jyotiphy.rsh@gndu.ac.in (J.); harpreetphy.rsh@gndu.ac.in (H.K.)
[2] Physical Research Laboratory, Atomic, Molecular and Optical Physics Division, Navrangpura, Ahmedabad 380009, Gujarat, India; bijaya@prl.res.in
* Correspondence: bindiya.phy@gndu.ac.in

Abstract: Light shift in a state due to the applied laser in an atomic system vanishes at tune-out wavelengths (λ_Ts). Similarly, differential light shift in a transition vanishes at the magic wavelengths (λ_{magic}s). In many of the earlier studies, values of the electric dipole (E1) matrix elements were inferred precisely by combining measurements and calculations of λ_{magic}. Similarly, the λ_T values of an atomic state can be used to infer the E1 matrix element, as it involves dynamic electric dipole (α) values of only one state whereas the λ_{magic} values require evaluation of α values for two states. However, both the λ_{magic} and λ_T values depend on angular momenta and their magnetic components (M) of states. Here, we report the λ_{magic} and λ_T values of many $S_{1/2}$ and $D_{3/2,5/2}$ states, and transitions among these states of the Mg^+, Ca^+, Sr^+ and Ba^+ ions that are independent of M values. It is possible to infer a large number of E1 matrix elements of the above ions accurately by measuring these values and combining with our calculations.

Keywords: relativistic all-order method; magic wavelength; tune-out wavelength; dipole polarizability

Citation: Jyoti; Kaur, H.; Arora, B.; Sahoo, B.K. Magnetic Sublevel Independent Magic and Tune-Out Wavelengths of the Alkaline-Earth Ions. *Atoms* **2022**, *10*, 72. https://doi.org/10.3390/atoms10030072

Academic Editor: Jean-Paul Mosnier

Received: 10 June 2022
Accepted: 6 July 2022
Published: 11 July 2022

1. Introduction

Singly charged alkaline-earth ions are the most eligible candidates for considering for high-precision measurements due to several advantages [1]. Except Be^+ and Mg^+, other alkaline-earth ions have two metastable states and most of the transitions among the ground and metastable states are accessible by lasers. This is why these ions are considered for carrying out high-precision measurements such as testing Lorentz symmetry violations [2–4], parity nonconservation effects [5], non-linear isotope shift effects [6], quantum information [7,8] and many more, including for the optical atomic clock experiments [9]. Above all, optical lattices blended with unique features of optical transitions in the ionic system lead to the revolution in the clock frequency states. Since the confinement of Mg^+ ions in a monochromatic optical dipole trap has become feasible experimentally for several ms [10], the pathways to implement these ions to realize optical lattice clocks have been opened up due to the fact that ions provide more accurate atomic clocks since various systematics in the ions can be controlled easily [11,12].

One of the major systematics in the aforementioned high-precision measurements is the Stark shift due to the employed laser, which depends on the frequency of the laser. The solution to this problem was suggested by Katori et al. [13], who proposed that the trapping laser can be tuned to wavelengths at which differential ac Stark shifts of the transitions can vanish [13]. These wavelengths were coined as magic wavelengths (λ_{magic}s) and are being popularly used in optical lattice clocks. The development of the technique to measure λ_{magic}s in the singly charged $^{40}Ca^+$ ion [14] has opened up the possibilities to measure these wavelengths in the other ions, such as Al^+, Hg^+, Yb^+, Cd^+, In^+ and so on, that are being considered in many high-precision measurements. Further, the infrared magic wavelength has been identified recently for all optical trapping of $^{40}Ca^+$ ion

clock [15]. The stability of optical lattices can be enhanced by optical cavities in various dimensions while availing the coordinated choice of λ_{magic}s [16] and state-dependent potentials [17], which can further be implemented in the all-optical confinement of these ions. In quantum state engineering [18], λ_{magic}s provide an opportunity to extract accurate values of oscillator strengths [19], which are particularly important for correct stellar modeling and analysis of spectral lines identified in the spectra of stars and other heavenly bodies so as to infer fundamental stellar parameters [20,21].

Apart from the magic trapping condition, where light shift in two internal states is identical, another well-known limiting case is where light shift in one state vanishes. This case is known as a tune-out condition [22]. Applications of such tune-out wavelengths (λ_T) lie in novel cooling techniques of atoms [23], selective addressing and manipulation of quantum states [24–26], precision measurement of atomic structures [27–32] and precise estimation of oscillator strength ratios [33]. Additionally, tune-out conditions are powerful tools for the evaporative cooling of optical lattices [34] and, hence, are important for experimental explorations.

In one of the experiments pertaining to magic wavelengths of alkaline-earth ions, Liu et al. demonstrated the existence of magic wavelengths for a single trapped $^{40}Ca^+$ ion [14], whereas Jiang et al. evaluated magic wavelengths of Ca^+ ions for linearly and circularly polarized light using the relativistic configuration interaction plus core polarization (RCICP) approach [35,36]. Recently, Chanu et al. proposed a model to trap Ba^+ ions by inducing an ac Stark shift using a 653 nm linearly polarized laser [37]. Kaur et al. reported magic wavelengths for $nS_{1/2} - nP_{1/2,3/2}$ and $nS_{1/2} - mD_{3/2,5/2}$ transitions in alkaline-earth-metal ions using linearly polarized light [16], whereas Jiang et al. located magic and tune-out wavelengths for Ba^+ ions using the RCICP approach [38]. Despite having a large number of applications, these magic wavelengths suffer a setback because of their dependency on the magnetic-sublevels (M) of the atomic systems. Linearly polarized light has been widely used for the trapping of atoms and ions as it is free from the contribution of the vector component in the interaction between atomic states and electric fields. However, the magic wavelengths thus identified are again magnetic-sublevel dependent for the transitions involving states with angular momenta greater than 1/2. On the other hand, the cooling of ions using circularly polarized light requires magnetic-sublevel selections. In order to circumvent this M dependency of magic wavelengths, a magnetic-sublevel-independent strategy for the trapping of atoms and ions was proposed by Sukhjit et al. [39]. Later on, Kaur et al. implemented a similar technique to compute magic and tune-out wavelengths independent of magnetic sublevels M for different $nS_{1/2} - (n-1)D_{3/2,5,2}$ transitions in Ca^+, Sr^+ and Ba^+ ions corresponding to n = 4 for Ca^+, 5 for Sr^+ and 6 for Ba^+ ion [40].

In addition to the applications of λ_{magic} in getting rid of differential Stark shift in a transition, they are also being used to infer the electric dipole (E1) matrix elements of many allowed transitions in different atomic systems [14,38,41,42]. The basic procedure of these studies is that the λ_{magic} values are calculated by fine-tuning of the magnitudes of dominantly contributing E1 matrix elements to reproduce their measured values. Then, the set of the E1 matrix elements that gives rise to the best matched λ_{magic} values are considered as the recommended E1 matrix elements. However, calculations of these λ_{magic} values of a transition demand the determination of the dynamic E1 polarizabilities (α) of both the states. In view of this, use of the λ_T values of a given atomic state can be advantageous, as they involve dynamic α values of only one state. Furthermore, both the λ_{magic} and λ_T values depend on angular momenta and their magnetic components (M) of atomic states. This requires evaluation of scalar, vector and tensor components of the α values for states with angular momenta greater than 1/2, which is very cumbersome. To circumvent this problem, we present here M-sublevel-independent λ_{magic} and λ_T values of many states and transitions involving a number of $S_{1/2}$ and $D_{3/2,5/2}$ states in the alkaline-earth metal ions from Mg^+ through Ba^+ that can be inferred to the E1 matrix elements more precisely. The basic idea behind this work is to use the calculated E1 matrix elements to predict the M-independent λ_{magic} and λ_T values of the above ions. Theoretical determinations

of these λ_{magic} and λ_T are very sensitive to the magnitudes of a few principal E1 matrix elements. When measurements of these quantities are available, by combining them with our calculations it is possible to fine tune the E1 matrix element values to higher precision. At this stage, our reported λ_{magic} and λ_T values will be useful to guide the experimentalists to carry out these measurements. The measurements can be achieved by setting up experiments suitably by fixing the polarization and quantization angles of the applied lasers. To validate our results for the transitions involving high-lying states, we compared the values of our λ_{magic} and λ_T values for the ground to the metastable states of the considered alkaline-earth ions with the previously reported values.

The paper is organized as follows: In Section 2, we provide underlying theory and Section 3 describes the method of evaluation of the calculated quantities. Section 4 discusses the obtained results, while concluding the study in Section 5. Unless we have stated explicitly, physical quantities are given in atomic units (a.u.).

2. Theory

The electric field $\mathcal{E}(r,t)$ associated with a general plane electromagnetic wave can be represented in terms of complex polarization vector $\hat{\chi}$ and the real wave vector **k** by the following expression [43]

$$\mathcal{E}(\mathbf{r},t) = \frac{1}{2}\mathcal{E}\hat{\chi}e^{-\iota(\omega t - \mathbf{k}.\mathbf{r})} + c.c., \tag{1}$$

where $c.c.$ is the complex conjugate of the preceding term. Assuming $\hat{\chi}$ to be real and adopting the coordinate system as presented in Figure 1, the polarization vector can be expressed as [39]

$$\hat{\chi} = e^{\iota\sigma}(cos\phi\ \hat{\chi}_{maj} + \iota\ sin\phi\ \hat{\chi}_{min}), \tag{2}$$

where $\hat{\chi}_{maj}$ and $\hat{\chi}_{min}$ denote the real components of the polarization vector $\hat{\chi}$, σ is the real quantity denoting the arbitrary phase and ϕ is analogous to degree of polarization A such that $A = sin(2\phi)$. For linearly polarized light, $\phi = 0$ whereas ϕ takes the value either $\pi/4$ or $3\pi/4$ for circularly polarized light, which further defines $A = 0$ for linearly polarized and $A = 1(-1)$ for right-hand (left-hand) circularly polarized light [43]. As shown in Figure 1, this coordinate system follows

$$cos^2\theta_p = cos^2\phi\ cos^2\theta_{maj} + sin^2\phi\ sin^2\theta_{min} \tag{3}$$

and

$$\theta_{maj} + \theta_{min} = \frac{\pi}{2}. \tag{4}$$

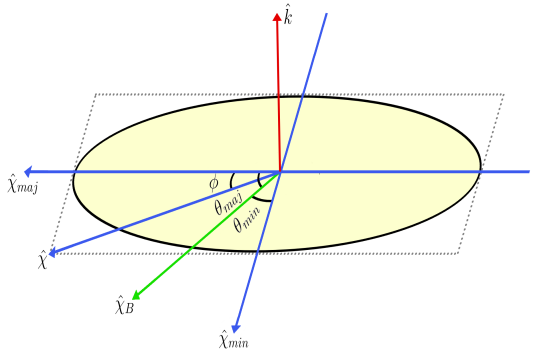

Figure 1. Representation of elliptically polarized laser beam swept out by the laser's polarization vector in one period. $\hat{\chi}$ represents the laser's complex polarization vector and $\hat{k}$ as the laser wave vector perpendicular to quantization axis $\hat{\chi}_B$. The vectors $\hat{\chi}_{maj}$, $\hat{\chi}_{min}$ and $\hat{k}$ are mutually perpendicular to each other.

Here, θ_p is the angle between quantization axis $\hat{\chi}_B$ and direction of polarization vector $\hat{\chi}$ and the parameters θ_{maj} and θ_{min} are the angles between respective unit vectors and $\hat{\chi}_B$.

When an atomic system is subjected to the above electric field and the magnitude of $\mathcal{E}$ is small, a shift in the energy of its n^{th} level (Stark shift) can be given by

$$\delta E_n^K \simeq -\frac{1}{2}\alpha_n^K(\omega)|\mathcal{E}|^2, \tag{5}$$

where $\alpha_n^K(\omega)$ is known as the second-order electric dipole (E1) polarizability and the superscript K denotes angular momentum of the state, which can be atomic angular momentum J or hyperfine-level angular momentum F. Depending upon polarization, dynamic dipole polarizability $\alpha_n^K(\omega)$ can be expressed as

$$\begin{aligned}\alpha_n^K(\omega) = \alpha_{nS}^K(\omega) + \beta(\chi)\tfrac{M_K}{2K}\alpha_{nV}^K(\omega)\\ +\gamma(\chi)\tfrac{3M_K^2-K(K+1)}{K(2K-1)}\alpha_{nT}^K(\omega),\end{aligned} \tag{6}$$

where α_{nS}^K, α_{nV}^K and α_{nT}^K are the scalar, vector and tensor components of the polarizability, respectively. The expression can be defined on the basis of the coordinate system provided in the Figure 1. Geometrically, values for $\beta(\chi)$ and $\gamma(\chi)$ in their elliptical form are given as [39,43]

$$\beta(\chi) = \iota(\hat{\chi}\times\hat{\chi}^*).\hat{\chi}_B = A cos\,\theta_k \tag{7}$$

and

$$\gamma(\chi) = \frac{1}{2}[3(\hat{\chi}^*.\hat{\chi}_B)(\hat{\chi}.\hat{\chi}_B) - 1] = \frac{1}{2}\Big(3cos^2\,\theta_p - 1\Big), \tag{8}$$

where θ_k is the angle between direction of propagation $\mathbf{k}$ and $\hat{\chi}_B$. Substitution of $\beta(\chi)$ and $\gamma(\chi)$ from Equations (7) and (8) reforms the expression for dipole polarizability to

$$\begin{aligned}\alpha_n^K(\omega) = \alpha_{nS}^K(\omega) + Acos\theta_k\tfrac{M_K}{2K}\alpha_{nV}^K(\omega)\\ +\left(\tfrac{3cos^2\theta_p-1}{2}\right)\tfrac{3M_K^2-K(K+1)}{K(2K-1)}\alpha_{nT}^K(\omega)\end{aligned} \tag{9}$$

with the azimuthal quantum number M_K of the respective angular momentum K.

Thus, it is obvious from Equation (6) that the α_n^K values of two states have to be same if we intend to find λ_{magic} for the transition involving both the states. Since the above expression for α_n^K has M_K dependency, the λ_{magic} become M_K dependent. In order to remove M_K dependency, one can choose $M_K = 0$ sublevels but in the atomic states of the alkaline-earth ions they are non-zero while isotopes with integer nuclear spin of the alkaline-earth ions M_Ks are again non-zero. To address this, a suitable combination of the $\beta(\chi)$ and $\gamma(\chi)$ parameters needs to be chosen such that $cos\theta_k = 0$ and $cos^2\theta_p = \frac{1}{3}$, which are feasible to achieve in an experiment by setting θ_k, $\hat{\chi}_{maj}$ and ϕ values, as demonstrated in Ref. [39]. In such a scenario, the λ_{magic} values can depend on the scalar part only by suppressing the vector and tensor components of α_n^K; i.e., the net differential Stark effect of a transition occurring from the J to J' states will be given by

$$\delta E_{JJ'} = -\frac{1}{2}\Big[\alpha_{nS}^J(\omega) - \alpha_{nS}^{J'}(\omega)\Big]\mathcal{E}^2. \tag{10}$$

This has an additional advantage that the differential Stark effects at an arbitrary electric field become independent of the choice of atomic or hyperfine levels in a given atomic system, as the scalar component of α_n^J and α_n^F are the same. Again, the same choice of λ_{magic} values will be applicable to both the atomic and hyperfine levels in a high-precision experiment.

3. Method of Evaluation

Determination of α_n^J values requires accurate calculations of E1 matrix elements. For the computation of E1 matrix elements, we need accurate atomic wave functions of the alkaline-earth ions. We employed here a relativistic all-order method to determine

the atomic wave functions of the considered atomic systems, whose atomic states have a closed-core configuration with an unpaired electron in the valence orbital. Detailed descriptions of our all-order method can be found in Refs. [44–47]; however, a brief outline of the same is also provided here for the completeness.

Our all-order method follows the relativistic coupled-cluster (RCC) theory ansätz

$$|\psi_v\rangle = e^S|\phi_v\rangle, \tag{11}$$

where $|\phi_v\rangle$ represents the mean-field wave function of the state v and constructed as [48]

$$|\phi_v\rangle = a_v^\dagger|0_c\rangle, \tag{12}$$

where $|0_c\rangle$ represents the Dirac–Hartree–Fock (DHF) wave function of the closed core. Subscript v represents the valence orbital of the considered state. In our calculations, we consider only linear terms in the singles and doubles approximation of the RCC theory (SD method) by expressing [48]

$$|\psi_v\rangle = (1 + S_1 + S_2 + ...)|\phi_v\rangle, \tag{13}$$

where S_1 and S_2 depict terms corresponding to the single and double excitations, respectively, that can further be written in terms of second quantization creation and annihilation operators as follows [49]

$$S_1 = \sum_{ma} \rho_{ma} a_m^\dagger a_a + \sum_{m \neq v} \rho_{mv} a_m^\dagger a_v \tag{14}$$

and

$$S_2 = \frac{1}{2} \sum_{mnab} \rho_{mnab} a_m^\dagger a_n^\dagger a_b a_a + \sum_{mna} \rho_{mnva} a_m^\dagger a_n^\dagger a_a a_v, \tag{15}$$

where indices m and n range over all possible virtual orbitals, and indices a and b range over all occupied core orbitals. The coefficients ρ_{ma} and ρ_{mv} represent excitation coefficients of the respective single excitations for the core and the valence electrons, respectively, whereas ρ_{mnab} and ρ_{mnva} depict double excitation coefficients for the core and the valence electrons, respectively. These amplitudes are calculated in an iterative procedure [50], due to which they include electron correlation effects to all-order.

Hence, atomic wave function of the considered states in the alkaline-earth ions are expressed as [48,51]:

$$\begin{aligned} |\psi_v\rangle_{SD} &= \Big[1 + \textstyle\sum_{ma} \rho_{ma} a_m^\dagger a_a + \frac{1}{2} \sum_{mnab} \rho_{mnab} a_m^\dagger a_n^\dagger a_b a_a \\ &\quad + \textstyle\sum_{m \neq v} \rho_{mv} a_m^\dagger a_v + \sum_{mna} \rho_{mnva} a_m^\dagger a_n^\dagger a_a a_v \Big] |\phi_v\rangle. \end{aligned} \tag{16}$$

To improve the calculations further and understand the importance of contributions from the triple excitations in the RCC theory, we take into account important core and valence triple excitations through the perturbative approach over the SD method (SDpT method) by redefining the wave function expression as [48]

$$\begin{aligned} |\psi_v\rangle_{SDpT} &= |\psi_v\rangle_{SD} + \Big[\frac{1}{6} \textstyle\sum_{mnrab} \rho_{mnrvab} a_m^\dagger a_n^\dagger a_r^\dagger a_b a_a a_v \\ &\quad + \frac{1}{18} \textstyle\sum_{mnrabc} \rho_{mnrabc} a_m^\dagger a_n^\dagger a_r^\dagger a_c a_b a_a \Big] |\phi_v\rangle. \end{aligned} \tag{17}$$

After obtaining the wave functions of the interested atomic states, we evaluate the E1 matrix elements between states $|\psi_v\rangle$ and $|\psi_w\rangle$ as [49]

$$D_{wv} = \frac{\langle\psi_w|D|\psi_v\rangle}{\sqrt{\langle\psi_w|\psi_w\rangle\langle\psi_v|\psi_v\rangle}}, \tag{18}$$

where $D = -e\Sigma_j \mathbf{r}_j$ is the E1 operator with $\mathbf{r}_j$ being the position of jth electron [51]. The resulting expression of numerator of Equation (18) includes the sum of the DHF matrix elements z_{wv}; twenty correlation terms of the SD method that are linear or quadratic functions of excitation coefficients ρ_{mv}, ρ_{ma}, ρ_{mnva} and ρ_{mnab}; and their core counterparts [45].

In the sum-over-states approach, expression for the scalar dipole polarizability is given by

$$\alpha_v(\omega) = \frac{2}{3(2J_v+1)} \sum_{v\neq w} \frac{(E_v - E_w)|\langle\psi_v||D||\psi_w\rangle|^2}{(E_v - E_w)^2 - \omega^2}, \tag{19}$$

where $\langle\psi_v||D||\psi_w\rangle$ is the reduced matrix element for the transition occurring between the states involving the valence orbitals v and w. Here, we dropped the superscript J in the dipole polarizability notation for the brevity. For convenience, we divide the entire contribution to $\alpha_n(\omega)$ for any state v, into three parts, as

$$\alpha_v = \alpha_{v,c} + \alpha_{v,vc} + \alpha_{v,val} \tag{20}$$

where c, vc and val corresponds to core, valence-core and valence contributions arising due to the correlations among the core orbitals, core-valence orbitals and valence-virtual orbitals, respectively [52]. Due to much smaller magnitudes, the core and core-valence contributions are calculated using the DHF method. The dominant contributions will arise valence from $\alpha_{v,val}$ due to small energy denominators. Again, the high-lying states will not contribute to $\alpha_{v,val}$ owing to large energy denominators. Thus, we calculate E1 matrix elements only among the low-lying excited states and refer the contributions as 'Main'. Contributions from the less contributing high-lying states are referred as 'Tail' and are estimated again using the DHF method. To reduce the uncertainties in the estimations of Main contributions, we used experimental energies of the states from the National Institute of Science and Technology atomic database (NIST AD) [53].

4. Results and Discussion

The precise computation of magic and tune-out wavelengths requires the accurate determination of E1 matrix elements as well as dipole polarizabilities. In our work, we used E1 matrix elements available on Portal for High-Precision Atomic Data and Computation [54] and NIST Atomic Spectra Database [53], respectively.

We listed resonance transitions, magic wavelengths and their corresponding polarizabilities along with their uncertainties for magnetic-sublevel independent $nS - mD$ transitions for alkaline-earth ions from Mg^+ through Ba^+ along with their comparison with the available literature in the Table 1 through Table 4, respectively. Results reported by Kaur et al. [40] were obtained by similar analyses, but contributions from some of the high-lying states were neglected in that work. Furthermore, we used excitation energies for most of the states listed in the NIST AD compared to Kaur et al. This resulted in more precise values of dipole polarizabilities, hence further improving the magic and tune-out wavelengths.

Table 1. Magic wavelengths λ_{magic} (in nm) with their corresponding polarizability $\alpha_n(\omega)$ (in a.u.) for $(3,4)S_{1/2} - 3D_{3/2,5/2}$ and $4S_{1/2} - 4D_{3/2}$ transitions in Mg^+ ion.

$3S_{1/2} - 3D_{3/2}$				$3S_{1/2} - 3D_{5/2}$			
Resonance	λ_{res}	λ_{magic}	α_{magic}	**Resonance**	λ_{res}	λ_{magic}	α_{magic}
$3D_{3/2} \rightarrow 6P_{3/2}$	292.92			$3D_{5/2} \rightarrow 5F_{5/2}$	310.56		
		313.89 (2)	168.72 (13)			313.86 (2)	168.85 (13)
$3D_{3/2} \rightarrow 5P_{1/2}$	385.15			$3D_{5/2} \rightarrow 5P_{3/2}$	384.920		
		385.300 (1)	73.51 (7)			385.101 (1)	73.59 (6)
		757.8 (1.5)	40.43 (5)				
$3D_{3/2} \rightarrow 5P_{3/2}$	1091.83			$3D_{5/2} \rightarrow 4F_{5/2}$	448.24		
		1092.436 (1)	37.41 (5)			756.7 (1.5)	40.45 (5)
$3D_{3/2} \rightarrow 4P_{1/2}$	1095.48			$3D_{5/2} \rightarrow 4P_{3/2}$	1091.72		
$4S_{1/2} - 3D_{3/2}$				$4S_{1/2} - 3D_{5/2}$			
$4S_{1/2} \rightarrow 5P_{3/2}$	361.48			$4S_{1/2} \rightarrow 5F_{7/2}$	310.56		
		361.26 (1)	−202.1 (1.3)			344.87 (47)	−160.00 (13)
$4S_{1/2} \rightarrow 5P_{1/2}$	361.66			$4S_{1/2} \rightarrow 5P_{3/2}$	361.48		
		361.627 (1)	−203.2 (1.3)			361.626 (1)	−203.8 (1.3)
$4S_{1/2} \rightarrow 4P_{3/2}$	922.08			$4S_{1/2} \rightarrow 5P_{1/2}$	361.66		
		923.812 (1)	−140.74 (97)				
$4S_{1/2} \rightarrow 4P_{1/2}$	924.68			$3D_{5/2} \rightarrow 5P_{3/2}$	384.93		
						385.408 (4)	−163.67 (13)
$3D_{3/2} \rightarrow 4P_{3/2}$	1091.83			$3D_{5/2} \rightarrow 4F_{5/2}$	448.24		
		1092.377 (1)	1976.9 (1.5)				
$3D_{3/2} \rightarrow 4P_{1/2}$	1095.48			$4S_{1/2} \rightarrow 4P_{3/2}$	922.08		
		1132.53 (6)	1681.4 (1.3)			923.812 (1)	−144.72 (98)
				$4S_{1/2} \rightarrow 4P_{1/2}$	924.68		
				$3D_{5/2} \rightarrow 4P_{3/2}$	1091.72		
						1128.42 (6)	1706.3 (1.3)
$4S_{1/2} - 4D_{3/2}$				$4S_{1/2} - 4D_{5/2}$			
$4D_{3/2} \rightarrow 7F_{5/2}$	526.58			$4D_{5/2} \rightarrow 7F_{5/2,7/2}$	526.57		
		591.48 (1)	−422.01 (31)			591.34 (1)	−421.69 (31)
$4D_{3/2} \rightarrow 7P_{3/2}$	591.83			$4D_{5/2} \rightarrow 7P_{3/2}$	591.81		
		591.8603 (3)	−422.86 (31)				
$4D_{3/2} \rightarrow 7P_{1/2}$	591.98						
		616.11 (22)	−482.44 (35)			616.02 (23)	−482.19 (35)
$4D_{3/2} \rightarrow 6F_{5/2}$	634.87			$4D_{5/2} \rightarrow 6F_{7/2}$	634.85		
$4P_{1/2} \rightarrow 4D_{3/2}$	787.92						
		789.499 (4)	−1578.9 (1.2)				
$4P_{3/2} \rightarrow 4D_{3/2}$	789.82			$4P_{3/2} \rightarrow 4D_{5/2}$	789.85		
$4D_{3/2} \rightarrow 6P_{3/2}$	811.78			$4D_{5/2} \rightarrow 6P_{3/2}$	811.75		
		811.8186 (1)	−1973.6 (1.5)			812.118 (1)	−1980.0 (1.5)
						844.63 (10)	−2964.8 (2.2)
$4D_{3/2} \rightarrow 6P_{1/2}$	812.83						
		812.648 (1)	−1991.3 (1.5)				
		843.61 (11)	−2921.4 (2.2)				
$4S_{1/2} \rightarrow 4P_{3/2}$	922.08			$4S_{1/2} \rightarrow 4P_{3/2}$	922.08		
		923.839 (1)	−4957.9 (6.5)			923.839 (1)	−4975.8 (6.4)
$4S_{1/2} \rightarrow 4P_{1/2}$	924.68			$4S_{1/2} \rightarrow 4P_{1/2}$	924.68		
$4D_{3/2} \rightarrow 5F_{5/2}$	963.51			$4D_{5/2} \rightarrow 5F_{7/2}$	963.45		
		1006.10 (13)	3585.5 (2.7)			1005.86 (13)	3594.8 (2.7)

Further discussion regarding the magic wavelengths is provided in the Section 4.1 for the considered alkaline-earth ions. Furthermore, we discussed our results for tune-out wavelengths in the Section 4.2 along with the comparison of our results with respect to the available theoretical data.

4.1. Magic Wavelengths

4.1.1. Mg^+

In Table 1, we tabulated our results for magic wavelengths and their corresponding dipole polarizabilities for $(3,4)S_{1/2} - 3D_{3/2,5/2}$ and $4S_{1/2} - 4D_{3/2}$ transitions. Figure 2a demonstrates scalar dipole polarizabilities of $3S_{1/2}$ and $3D_{3/2,5/2}$ states of Mg^+ ion with respect to the wavelength of the external field. It can be perceived from the figure that a number of magic wavelengths at the crossings of the scalar polarizabilities' curves of the corresponding state have been predicted for the transition. As can be seen from Table 1, a total of 4 magic wavelengths were found for $3S - 3D_{3/2}$ transition, whereas the $3S - 3D_{5/2}$

transition shows a total of 3 magic wavelengths in the range 300–1250 nm, out of which no magic wavelength was found to exist in visible spectrum. However, all the magic wavelengths enlisted in Table 1 support red-detuned trap.

Figure 2b represents the plot of scalar dipole polarizabilities of $4S$ and $4D_{3/2,5/2}$ states against the wavelength of the external field. It can also be assessed from Table 1 that there exists a total of nine magic wavelengths in the considered wavelength range for $4S - 4D_{3/2}$ transition, whereas only five magic wavelengths are seen for the $4S - 4D_{5/2}$ transition. However, in both cases, all the magic wavelengths except those around 616 nm, 844 nm and 1006 nm are close to resonance, thereby making them unsuitable for further use. However, out of these three values, λ_{magic} at 616 nm lies in the visible region and is far-detuned with considerable deep potential. Hence, we recommend this magic wavelength for the trapping of Mg^+ ions for both $4S$–$4D_{3/2,5/2}$ transitions for further experimentations in optical clock applications.

Figure 2c demonstrates the magic wavelengths for the M_J-independent scheme for $4S$–$3D_{3/2,5/2}$ transitions for Mg^+ ions along with their corresponding scalar dynamic polarizabilities. According to Table 1, it can be realized that none of the magic wavelengths for these transitions lie within the visible spectrum of electromagnetic radiations. However, all of these magic wavelengths support a red-detuned trap, except 1132.53(6) nm and 1128.42(6) nm for $4S$-$3D_{3/2}$ and $4S - 3D_{5/2}$ transitions, respectively, support far blue-detuned traps and are found to be useful for experimental demonstrations.

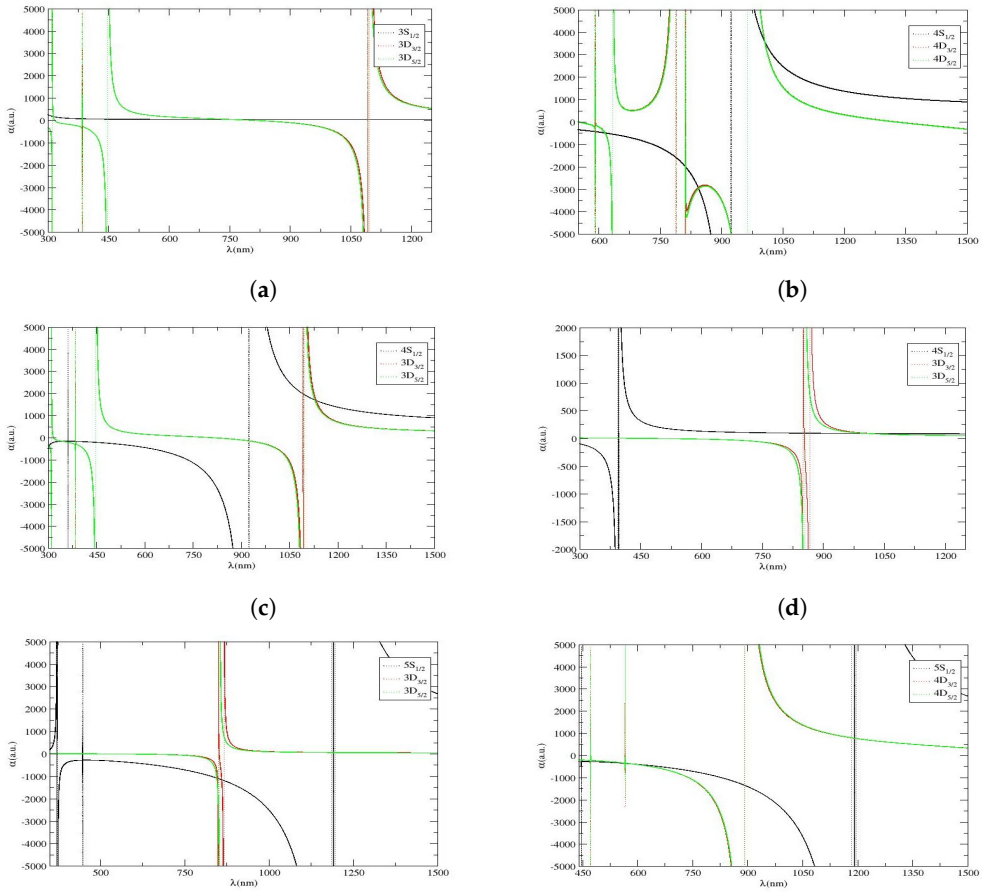

(**a**) (**b**)

(**c**) (**d**)

(**e**) (**f**)

Figure 2. α v/s λ plots for various transitions in Mg^+ and Ca^+ ions. (**a**) α v/s λ plot for $3S_{1/2} - 3D_{3/2,5/2}$ transition in Mg^+ ion. (**b**) α v/s λ plot for $4S_{1/2} - 4D_{3/2,5/2}$ transition in Mg^+ ion. (**c**) α v/s λ plot for $4S_{1/2} - 3D_{3/2,5/2}$ transition in Mg^+ ion. (**d**) α v/s λ plot for $4S_{1/2} - 3D_{3/2,5/2}$ transition in Ca^+ ion. (**e**) α v/s λ plot for $5S_{1/2} - 3D_{3/2,5/2}$ transition in Ca^+ ion. (**f**) α v/s λ plot for $5S_{1/2} - 4D_{3/2,5/2}$ transition in Ca^+ ion.

4.1.2. Ca^+

We considered $4S - 3D_{3/2,5/2}$ and $5S - (4,3)D_{3/2,5/2}$ transitions for locating the magic wavelengths in Ca^+ ion. We tabulated magic wavelengths for these transitions along with the comparison of λ_{magic}s with the only available results for $4S - 3D_{3/2,5/2}$ in Table 2. In addition, we plotted scalar dipole polarizabilities against wavelengths for these transitions in Figure 2d–f, correspondingly. According to Table 2, it is determined that, subsequently, three and two magic wavelengths exist between 393 nm and 1030 nm for $4S - 3D_{3/2,5/2}$ transitions. In both cases, except 1029.0(1.2) nm and 1011.90(90) nm magic wavelengths, which are far-detuned, all other magic wavelengths are close to resonances and are not suitable for laser trapping.

During analysis, six and five magic wavelengths were located for the $5S - (3,4)D_{3/2}$ and $5S - (3,4)D_{5/2}$ transitions, respectively. It was also determined that all the magic wavelengths are approximately same for both $5S - 4D_{3/2}$ and $5S - 4D_{5/2}$ transitions. Moreover, λ_{magic}s around 845 nm, 847 nm and 860 nm share deep trapping potential for blue-detuned traps and, hence, are further recommended for configuring feasible traps. λ_{magic} at 1191.56 nm, identified in the infrared region for both $5S - 4D_{3/2,5/2}$ transitions, is the only magic wavelength that supports the red-detuned trap. In addition, the polarizability for this wavelength is sufficient enough for creating an ion trap at reasonable laser power. To validate our results, we also compared our results with the results provided only for $4S - 3D_{3/2,5/2}$ in Ref. [40], and noticed that the results for these transitions are in good agreement with only less than 1% variation w.r.t. obtained results.

Table 2. Magic wavelengths λ_{magic} (in nm) with their corresponding polarizability $\alpha_n(\omega)$ (in a.u.) for $(4,5)S_{1/2} - 3D_{3/2,5/2}$ and $5S_{1/2} - 4D_{3/2,5/2}$ transitions in Ca^+ ion and their comparison with the available literature.

$4S_{1/2} - 3D_{3/2}$				$4S_{1/2} - 3D_{5/2}$			
Resonance	λ_{res}	λ_{magic}	α_{magic}	**Resonance**	λ_{res}	λ_{magic}	α_{magic}
$4S_{1/2} \rightarrow 4P_{3/2}$	393.48			$4S_{1/2} \rightarrow 4P_{3/2}$	393.47		
		395.795 (3)	5.6 (1.6)			395.795 (3)	5.6 (1.6)
		395.82 (3) [40]	4.90 [40]			395.82 (2) [40]	95.87 [40]
$4S_{1/2} \rightarrow 4P_{1/2}$	396.96			$4S_{1/2} \rightarrow 4P_{1/2}$	396.96		
$3D_{3/2} \rightarrow 4P_{3/2}$	850.04			$3D_{5/2} \rightarrow 4P_{3/2}$	854.44		
		852.42 (2)	95.67 (26)			1011.90 (90)	88.89 (25)
		852.45 (2) [40]	4.20 [40]			1014.10 (3) [40]	89.01 [40]
$3D_{3/2} \rightarrow 4P_{1/2}$	866.45						
		1029.0 (1.2)	88.39 (25)				
		1029.7 (2) [40]	88.55 [40]				
$5S_{1/2} - 3D_{3/2}$				$5S_{1/2} - 3D_{5/2}$			
$4P_{1/2} \rightarrow 5S_{1/2}$	370.71			$4P_{1/2} \rightarrow 5S_{1/2}$	370.71		
		371.76 (1)	6.7 (1.6)			371.76 (1)	6.7 (1.6)
$4P_{3/2} \rightarrow 5S_{1/2}$	373.80			$4P_{3/2} \rightarrow 5S_{1/2}$	373.80		
$5S_{1/2} \rightarrow 6P_{3/2}$	447.33			$5S_{1/2} \rightarrow 6P_{3/2}$	447.33		
		447.385 (5)	3.0 (1.6)			447.385 (5)	2.9 (1.6)
$5S_{1/2} \rightarrow 6P_{1/2}$	448.07			$5S_{1/2} \rightarrow 6P_{1/2}$	448.07		
		448.088 (2)	2.9 (1.6)			448.088 (2)	2.9 (1.6)
		847.69 (2)	−1089.4 (2.8)			845.78 (4)	−1079.8 (2.8)
$3D_{3/2} \rightarrow 4P_{3/2}$	850.04			$3D_{5/2} \rightarrow 4P_{3/2}$	854.44		
		860.22 (7)	−1154.7 (3.0)				
$3D_{3/2} \rightarrow 4P_{1/2}$	866.45						
$5S_{1/2} \rightarrow 5P_{3/2}$	1184.22			$5S_{1/2} \rightarrow 5P_{3/2}$	1184.22		
		1191.59 (1)	58.9 (1.6)		1191.59 (1)		56.8 (1.5)
$5S_{1/2} \rightarrow 5P_{1/2}$	1195.30			$5S_{1/2} \rightarrow 5P_{1/2}$	1195.30		
$5S_{1/2} - 4D_{3/2}$				$5S_{1/2} - 4D_{5/2}$			
$5S_{1/2} \rightarrow 6P_{3/2}$	447.33			$5S_{1/2} \rightarrow 6P_{3/2}$	447.34		
		447.52 (2)	−204.2 (2.4)			447.52 (2)	−205.3 (2.4)
$5S_{1/2} \rightarrow 6P_{1/2}$	448.07			$5S_{1/2} \rightarrow 6P_{1/2}$	448.07		
		448.16 (2)	−204.7 (2.4)			448.16 (1)	−205.8 (2.4)
		471.22 (24)	−279.71 (85)			471.67 (23)	−279.85 (85)
$4D_{3/2} \rightarrow 5F_{5/2}$	471.81			$4D_{5/2} \rightarrow 5F_{5/2,7/2}$	472.23		
		565.51 (2)	−355.55 (91)			566.03 (13)	−356.17 (92)
$4D_{3/2} \rightarrow 6P_{3/2}$	565.53			$4D_{5/2} \rightarrow 6P_{3/2}$	566.15		
		566.67 (17)	−356.93 (92)				
$4D_{3/2} \rightarrow 6P_{1/2}$	566.71						
$4D_{3/2} \rightarrow 4F_{5/2}$	891.45			$4D_{5/2} \rightarrow 4F_{7/2}$	892.98		
$5S_{1/2} \rightarrow 5P_{3/2}$	1184.22			$5S_{1/2} \rightarrow 5P_{3/2}$	1184.22		
		1191.56 (1)	776.1 (8.1)			1191.56 (1)	779.9 (7.9)
$5S_{1/2} \rightarrow 5P_{1/2}$	1195.30			$5S_{1/2} \rightarrow 5P_{1/2}$	1195.302		

4.1.3. Sr^+

Figure 3a–c demonstrate M_J-independent dynamic dipole polarizability versus wavelength plots for $(6,5)S_{1/2} - 4D_{3/2,5/2}$ and $6S_{1/2} - 5D_{3/2,5/2}$ transitions for Sr^+ ion. The results corresponding to these figures are listed in Table 3. Only two magic wavelengths were traced for the $5S - 4D_{3/2}$ transition, whereas only one magic wavelength exists for the $5S - 4D_{5/2}$ transition. According to Table 3, for the $6S - 4D_{3/2}$ transition, three magic wavelengths exist below 480 nm, with a dynamic polarizability of value less than 15 a.u.; however, another three λ_{magic}s, lie between 1000 nm and 1231 nm. The λ_{magic}s at 1002.401 nm and 1087.35 nm support blue-detuned traps with sufficiently high polarizabilities for the experimental trapping of Sr^+ ions. For the $6S - 4D_{5/2}$ transition, five magic wavelengths were located between 420 nm and 1250 nm, out of which the magic wavelengths at 421.47(5) nm, 474.61(1) nm, 477.549(0) nm and 1230.05(6) nm follow red-detuned traps, whereas the only magic wavelength at 1025.19(17) nm, with corresponding $\alpha = -2858.0(8.8)$ a.u., supports a blue-detuned trap, which can be useful for experimental purposes. We recommend this magic wavelength of Sr^+ ion for the $6S$-$4D_{5/2}$ transition. Moreover, it is also observed that all the magic wavelengths for these two transitions lie between the same resonance transitions and are closer to each other. Threfore, it is probable to trap Sr^+ ion for both of these transitions with same magic wavelength.

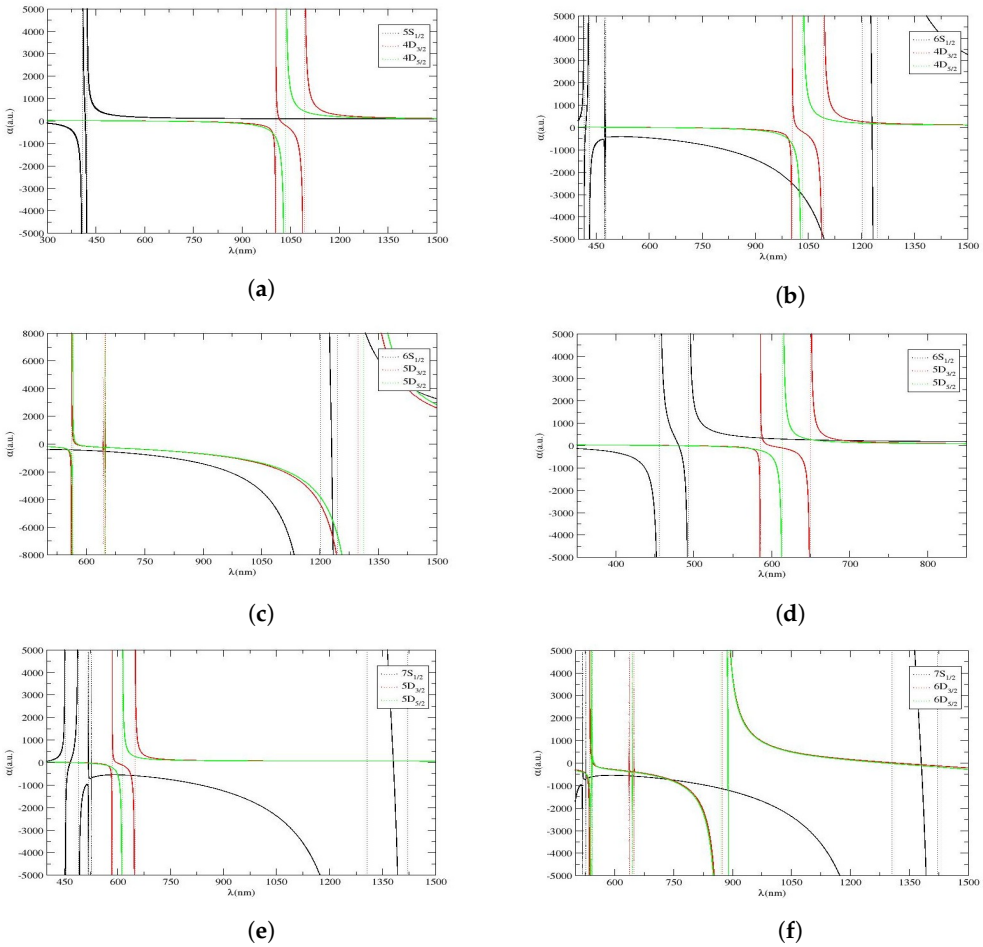

(**a**) (**b**) (**c**) (**d**) (**e**) (**f**)

Figure 3. α v/s λ plots for various transitions in Sr^+ and Ba^+ ions. (**a**) α v/s λ plot for $5S_{1/2}$ and $4D_{3/2,5/2}$ states of Sr^+ ion. (**b**) α v/s λ plot for $6S_{1/2} - 4D_{3/2,5/2}$ transition in Sr^+ ion. (**c**) α v/s λ plot for $6S_{1/2} - 5D_{3/2,5/2}$ transition in Sr^+ ion. (**d**) α v/s λ plot for $6S_{1/2} - 5D_{3/2,5/2}$ transition in Ba^+ ion. (**e**) α v/s λ plot for $7S_{1/2} - 5D_{3/2,5/2}$ transition in Ba^+ ion. (**f**) α v/s λ plot for $7S_{1/2} - 6D_{3/2,5/2}$ transition in Ba^+ ion.

Table 3 also shows that there are four magic wavelengths that lie within the wavelength range of 640 nm to 1450 nm for the $6S - 5D_{3/2}$ transition. It is also observed that three out of four magic wavelengths for $6S - 5D_{3/2}$ transition support blue-detuned traps; however, the $\lambda_{magic} = 1233.61(5)$ nm at $\alpha_{magic} = -6756(24)$ a.u. is recommended for experimental purposes as it is far-detuned and a high value of dipole polarizability indicates deep trapping potential. On the other hand, only three magic wavelengths were identified for the $6S - 5D_{5/2}$ transition in Sr^+ ion with two supporting blue-detuned traps. Two out of these λ_{magic}s, i.e., 1233.06(5) nm and 1448.4(1.6) nm, are located at higher wavelength ranges, with deep potentials for their respective favourable blue- and red-detuned traps. Therefore, both of these values are recommended for further experimental studies. Moreover, we compared our magic wavelengths for $5S - 4D_{3/2,5/2}$ transitions with respect to the available literature in the same table. It is seen that our reported values are in excellent approximation with the results obtained by Kaur et al. [40], with a variation by less than 0.05%. Unfortunately, we could not find any data related to other transitions to carry out the comparison with. Hence, it can be concluded from the comparison of available data that our results are promising and can be used for further prospective calculations of atomic structures and atomic properties of this ion.

Table 3. Magic wavelengths λ_{magic} (in nm) with their corresponding polarizability $\alpha_n(\omega)$ (in a.u.) along with their comparison with the available literature for $(5,6)S_{1/2} - 4D_{3/2,5/2}$ and $6S_{1/2} - 5D_{3/2,5/2}$ transitions in Sr^+ ion.

$5S_{1/2} - 4D_{3/2}$				$5S_{1/2} - 4D_{5/2}$			
Resonance	λ_{res}	λ_{magic}	α_{magic}	**Resonance**	λ_{res}	λ_{magic}	α_{magic}
$5S_{1/2} \rightarrow 5P_{3/2}$	407.89			$5S_{1/2} \rightarrow 5P_{3/2}$	407.89		
		417.00 (5)	15.3 (2.1)			417.00 (4)	15.2 (2.1)
		416.9 (3) [40]	14.47 [40]			416.9 (3) [40]	13.3 [40]
$5S_{1/2} \rightarrow 5P_{1/2}$	421.67			$5S_{1/2} \rightarrow 5P_{1/2}$	421.67		
$4D_{3/2} \rightarrow 5P_{3/2}$	1003.94			$4D_{5/2} \rightarrow 5P_{3/2}$	1003.01		
		1014.68 (26)	108.70 (90)				
		1014.6 (2) [40]	108.35 [40]				
$4D_{3/2} \rightarrow 5P_{1/2}$	1091.79						
$6S_{1/2} - 4D_{3/2}$				$6S_{1/2} - 4D_{5/2}$			
$5P_{1/2} \rightarrow 6S_{1/2}$	416.27			$5P_{1/2} \rightarrow 6S_{1/2}$	416.30		
		421.47 (5)	15.0 (2.1)			421.47 (5)	14.9 (2.1)
$5P_{3/2} \rightarrow 6S_{1/2}$	430.67			$5P_{3/2} \rightarrow 6S_{1/2}$	430.67		
$6S_{1/2} \rightarrow 7P_{3/2}$	474.37			$6S_{1/2} \rightarrow 7P_{3/2}$	474.37		
		474.61 (1)	11.3 (2.1)			474.61 (1)	10.9 (2.1)
$6S_{1/2} \rightarrow 7P_{1/2}$	477.49			$6S_{1/2} \rightarrow 7P_{1/2}$	477.49		
		477.549 (0)	11.1 (2.1)			477.557 (5)	10.7 (2.1)
		1002.40 (3)	−2470.0 (7.5)			1025.19 (17)	−2858.0 (8.8)
$4D_{3/2} \rightarrow 5P_{3/2}$	1003.94			$4D_{5/2} \rightarrow 5P_{3/2}$	1033.01		
		1087.35 (9)	−4653 (15)				
$4D_{3/2} \rightarrow 5P_{1/2}$	1091.79			$6S_{1/2} \rightarrow 6P_{3/2}$	1201.73		
$6S_{1/2} \rightarrow 6P_{3/2}$	1201.73					1230.05 (6)	170.2 (3.6)
		1230.02 (6)	223.4 (4.2)				
$6S_{1/2} \rightarrow 6P_{1/2}$	1244.84			$6S_{1/2} \rightarrow 6P_{1/2}$	1244.84		
$6S_{1/2} - 5D_{3/2}$				$6S_{1/2} - 5D_{5/2}$			
$5D_{3/2} \rightarrow 5F_{5/2}$	562.45			$5D_{5/2} \rightarrow 5F_{5/2}$	565.20		
		643.871 (2)	−528.6 (1.5)			647.41 (2)	−534.6 (1.6)
$5D_{3/2} \rightarrow 7P_{3/2}$	643.88			$5D_{5/2} \rightarrow 7P_{3/2}$	647.49		
		649.49 (2)	−538.2 (1.6)				
$5D_{3/2} \rightarrow 7P_{1/2}$	649.65						
$6S_{1/2} \rightarrow 6P_{3/2}$	1201.73			$6S_{1/2} \rightarrow 6P_{3/2}$	1201.73		
		1233.61 (5)	−6756 (29)			1233.06 (5)	−5620 (23)
$6S_{1/2} \rightarrow 6P_{1/2}$	1244.84			$6S_{1/2} \rightarrow 6P_{1/2}$	1244.84		
$5D_{3/2} \rightarrow 4F_{5/2}$	1297.85			$5D_{5/2} \rightarrow 4F_{5/2}$	1312.62		
		1411.9 (1.5)	4382 (13)				
				$5D_{5/2} \rightarrow 4F_{7/2}$	1312.84		
						1448.4 (1.6)	3812 (11)

4.1.4. Ba^+

The results for magic wavelengths for $6S - 5D_{3/2,5/2}$, $7S - 5D_{3/2,5/2}$ and $7S - 6D_{3/2,5/2}$ transitions in Ba^+ ion are tabulated in Table 4. As per Figure 3d and Table 4, a maximum number of magic wavelengths were located between 480 and 700 nm. It is also observed that the magic wavelengths that lie between $6S - 6P_{1/2}$ and $6S - 6P_{3/2}$ resonant transitions support blue-detuned trap; however, the dynamic dipole polarizability corresponding to these magic wavelengths are too small to trap Ba^+ ions at these wavelengths. A total of

six magic wavelengths were found for the $7S - 5D_{3/2}$ transition, out of which two lie in the vicinity of 526 nm. The sharp intersection of the polarizability curves of the involved states of transition lie at 583.76(1) nm, 638.75(5) nm and 1380.83(24) nm. Similarly, four magic wavelengths were identified for the $7S - 5D_{5/2}$ transition; however, unlike the $7S - 5D_{3/2}$ transition, no magic wavelength was identified in the vicinity of 600 to 1300 nm. It was also determined that three out of these four λ_{magic}s, support a blue-detuned trap, although the trapping potentials for these traps are not deep enough for further consideration in experimentations.

Table 4. Magic wavelengths λ_{magic} (in nm) with their corresponding polarizability α_n (ω) (in a.u.) along with their comparison with the available literature for $(6,7)S_{1/2} - 5D_{3/2,5/2}$ and $7S_{1/2} - 6D_{3/2,5/2}$ transitions in Ba^+ ions.

$6S_{1/2} - 5D_{3/2}$				$6S_{1/2} - 5D_{5/2}$			
Resonance	λ_{res}	λ_{magic}	α_{magic}	**Resonance**	λ_{res}	λ_{magic}	α_{magic}
$6S_{1/2} \rightarrow 6P_{3/2}$	455.53	480.71 (2) 480.6 (5) [40]	−4.1 (1.6) −2.89 [40]	$6S_{1/2} \rightarrow 6P_{3/2}$	455.53	480.76 (2)	−8.3 (1.4)
$6S_{1/2} \rightarrow 6P_{1/2}$	493.55			$6S_{1/2} \rightarrow 6P_{1/2}$	493.55		
$5D_{3/2} \rightarrow 6P_{3/2}$	585.53	588.32 (1) 588.4 (3) [40]	330.15 (60) 329.33 [40]	$5D_{3/2} \rightarrow 6P_{3/2}$	614.34	653.17 ()35 695.7 (3) [40]	247.90 (57) 219.4 [40]
$5D_{3/2} \rightarrow 6P_{1/2}$	649.87	693.46 (48) 655.50 (3) [40]	221.91 (56) 244.89 [40]				
$7S_{1/2} - 5D_{3/2}$				$7S_{1/2} - 5D_{5/2}$			
$6P_{1/2} \rightarrow 7S_{1/2}$	452.62	466.95 (13)	0.5 (1.6)	$6P_{1/2} \rightarrow 7S_{3/2}$	452.62	466.88 (9)	−2.6 (1.5)
$6P_{3/2} \rightarrow 7S_{1/2}$	490.13			$6P_{3/2} \rightarrow 7S_{1/2}$	490.13		
$7S_{1/2} \rightarrow 8P_{3/2}$	518.49	518.79 (2)	−22.9 (1.5)	$7S_{1/2} \rightarrow 8P_{3/2}$	518.49	518.79 (2)	−31.9 (1.5)
$7S_{1/2} \rightarrow 8P_{1/2}$	526.75	526.779 (6) 583.76 (1)	−28.7 (1.5) −548.6 (2.4)	$7S_{1/2} \rightarrow 8P_{1/2}$	526.75	601.37 (6)	−548.8 (1.6)
$5D_{3/2} \rightarrow 6P_{3/2}$	585.53	638.75 (5)	−573.9 (2.4)	$5D_{5/2} \rightarrow 6P_{3/2}$	614.34		
$5D_{3/2} \rightarrow 6P_{1/2}$	649.87						
$7S_{1/2} \rightarrow 7P_{3/2}$	1306.14	1380.83 (24)	59.8 (1.4)	$7S_{1/2} \rightarrow 7P_{3/2}$	1306.14	1380.83 (24)	59.2 ()1.3
$7S_{1/2} \rightarrow 7P_{1/2}$	1421.54			$7S_{1/2} \rightarrow 7P_{1/2}$	1421.54		
$7S_{1/2} - 6D_{3/2}$				$7S_{1/2} - 6D_{5/2}$			
$7S_{1/2} \rightarrow 8P_{3/2}$	518.49	519.03 (11)	−376 (34)	$7S_{1/2} \rightarrow 8P_{3/2}$	518.49	519.07 (10)	−405 (31)
$7S_{1/2} \rightarrow 8P_{1/2}$	526.750	526.84 (12) 531.0 (1.0)	−483 (43) −664.2 (4.0)	$7S_{1/2} \rightarrow 8P_{1/2}$	526.75	526.84 (6) 532.8 (2.4)	−480 (43) −655.2 (3.8)
$6D_{3/2} \rightarrow 6F_{5/2}$	536.28			$6D_{5/2} \rightarrow 6F_{7/2}$	539.31	542.17 (7)	−613.1 (3.2)
				$6D_{5/2} \rightarrow 6F_{5/2}$	542.26	645.33 (10)	−580.8 (2.5)
$6D_{3/2} \rightarrow 8P_{3/2}$	637.25			$6D_{5/2} \rightarrow 8P_{3/2}$	645.70	735.65 (92)	−728.3 (3.2)
$6D_{3/2} \rightarrow 8P_{1/2}$	649.77	744.0 (2.2)	−746.4 (3.2)	$6D_{5/2} \rightarrow 5F_{7/2}$	871.32	889.20 (20)	−1211.6 (5.5)
$6D_{3/2} \rightarrow 5F_{5/2}$	874.02			$6D_{5/2} \rightarrow 5F_{5/2}$	889.99		
$7S_{1/2} \rightarrow 7P_{3/2}$	1306.14	1381.25 (35)	−78 (77)	$7S_{1/2} \rightarrow 7P_{3/2}$	1306.14	1381.39 (33)	−125 (77)
$7S_{1/2} \rightarrow 7P_{1/2}$	1421.54			$7S_{1/2} \rightarrow 7P_{1/2}$	1421.54		

Table 4 also compiles the magic wavelengths for $7S - 5D_{3/2,5/2}$ transitions and shows that there exists six and four magic wavelengths for $7S - 5D_{3/2}$ and $7S - 5D_{5/2}$ transition, respectively. It is also seen that the magic wavelengths between $6P_{3/2} - 7S$ and $7S - 8P_{3/2}$ as well as the $5D_{3/2} - 6P_{1/2}$ and $7S - 7P_{3/2}$ transitions seem to be missing, as shown in Figure 3e. It is also observed that the magic wavelength at 466.95(13) nm and 1380.83(24) nm are slightly red-shifted; nevertheless, the λ_{magic} at 638.75(5) nm in the visible region supports a blue-detuned trap, and can have sufficient trap depth at reasonable laser power.

Similarly, the magic wavelengths and their corresponding dynamic dipole polarizability along with their comparison with available literature is also provided in the same table for $7S - 6D_{3/2,5/2}$ transitions. The same was demonstrated graphically in Figure 3f, which includes a total of thirteen magic wavelengths in all for the considered transitions. It is

also examined that no magic wavelength exists between $6D_{3/2} - 6F_{5/2}$ and $6D_{3/2} - 8P_{1/2}$ resonances. Unlike the $7S - 6D_{3/2}$ transition, around eight magic wavelengths were located between $7S - 8P_{3/2}$ and $7S - 7P_{1/2}$ resonances, and all of them support blue-detuned traps. Moreover, magic wavelengths at 532.8(2.4) nm, 735.65(92) nm and 1381.39(33) nm are expected to be more promising for experiments due to sufficient trap depths for reasonable-power lasers. However, on the comparison of our results for $6S - 5D_{3/2,5/2}$ transitions for Ba^+ ion, we observed that all the magic wavelengths agree well with the results obtained by Kaur et al., in Ref. [40], except the last magic wavelengths that were identified at 693 nm and 653 nm for $6S - 5D_{3/2}$ and $6S - 5D_{5/2}$ transitions.

4.2. Tune-Out Wavelengths

We illustrated tune-out wavelengths for different states of the considered transitions in the alkaline-earth ions along with their comparison with the already available literature in Table 5. To locate these M_J-independent tune-out wavelengths, we evaluated the scalar dipole dynamic polarizabilities of these states for considered alkaline-earth ions and identified those values of λ for which polarizability vanished. It is also highlighted that, in Mg^+ ion, all the tune-out wavelengths identified for $3S_{1/2}$ and $4S_{1/2}$ states lie in the UV region, whereas, for $(3,4)D_{3/2,5/2}$ states, a few tune-out wavelengths are located in visible range. Moreover, the largest λ_T is identified for the $4D_{3/2}$ state at 1331.53(53) nm. Furthermore, only one tune-out wavelength, i.e., $\lambda_T = 280.1136(2)$ nm for $3S_{1/2}$, could be compared with the result presented by Kaur et al. in Ref. [55] and it is seen that our result is in good accord with this value.

Similarly, we pointed out tune-out wavelengths for $nS_{1/2}$ and $(n-1)D_{3/2}$, $n = (4,5)$, $(5,6)$ and $(6,7)$ states for Ca^+, Sr^+ and Ba^+ ions, by identifying λs at which their corresponding αs tend to zero. Hence, it was perceived that, out of 25 tune-out wavelengths for all states of Ca^+ ion, only seven of them lie within visible spectrum and, on comparison of different tune-out wavelengths for the $4S_{1/2}$ and $3D_{3/2}$ states of Ca^+ ion, it was determined that all of these results are supported by the results obtained in Refs. [40,55]. However, one of the tune-out wavelength located at 493.13(87) nm for the $3D_{5/2}$ state of Ca^+ ion seems have 2% variation from the wavelength obtained by Kaur et al. in Ref. [40]. This results from the fact that the present study incorporates more precise E1 matrix elements for the high-lying transitions as well their excitation energies from the portal for High-Precision Atomic Data and Computation [54].

For Sr^+ ion, the maximum number of tune-out wavelengths was identified out of all the considered alkaline-earth ions. It is also realized that most of these λs lie within the visible spectrum of electromagnetic radiation, and are mostly comprised of all the λ_T values corresponding to $5S_{1/2}$, $5D_{3/2}$ and $5D_{5/2}$ states. Additionally, during the comparison of these values with the results published in Refs. [40,55], it was determined that the tune-out wavelength at 417.04(6) nm for $5S_{1/2}$ as well as $\lambda_T = 1018.91(38)$ nm for the $4D_{3/2}$ state agree well with the available results; howsoever, the tune-out wavelengths at 606.47(53) nm and 593.0(2.0) nm for $4D_{3/2}$ and $4D_{5/2}$ states, respectively, show a discrepancy of less than 2%, which lies within the error bar of 5%.

In the case of Ba^+ ion, we located 23 tune-out wavelengths, which, in all, comprise of 10, 9 and 4 wavelengths in visible, UV and infrared regions, respectively. It is also highlighted that all the tune-out wavelengths that exist in visible region lie within the range 480 nm to 550 nm. We also compared our tune-out wavelengths for $6S_{1/2}$ and $5D_{3/2,5/2}$ states against available theoretical data in Refs. [38,40,55] and it was found that all the λ_Ts except 468.61 nm and 459.57 nm, respectively, for $5D_{3/2}$ and $5D_{5/2}$ states show disparities of less than 1%, which lies within the considerable error limit.

Table 5. Tune-out wavelengths λ_T (in nm) of various states of Mg^+, Ca^+, Sr^+ and Ba^+ ions and their comparison with available literature.

Mg^+			Ca^+			Sr^+			Ba^+		
State	λ_T	**Others**	**State**	λ_T	**Others**	**State**	λ_T	**Others**	**State**	λ_T	**Others**
$3S_{1/2}$	102.6058 (6)		$4S_{1/2}$	165.04 (3)		$5S_{1/2}$	417.04 (5)	417.04 (6) [55] 417.025 [40]	$6S_{1/2}$	200.035 (1)	
	102.696 (8)			165.26 (4)							
	124.071 (7)			395.796 (3)	395.80 (2) [55] 395.796 [40]					202.51 (9)	
	280.1136 (2)	280.110 (9) [55]								480.66 (2)	480.63 (24) [55] 480.66 (18) [38] 480.596 [40]
$3D_{3/2}$	317.082 (59)		$3D_{3/2}$	212.930 (5)		$4D_{3/2}$	185.498 (2)		$5D_{3/2}$	224.675 (6)	
	384.9615 (4)			213.25 (2)			192.95 (95)			468.61 (61)	472.461 [40]
	385.3401 (9)			494.37 (63)	492.752 [40]		242.622 (7)			597.93 (15)	597.983 [40]
	812.03 (97)			852.75 (3)	852.776 [40]		606.47 (53)	598.633 [40]			
	1092.436 (9)						1018.91 (38)	1018.873 [40]			
$3D_{5/2}$	317.003 (6)		$3D_{5/2}$	170.63 (63)		$4D_{5/2}$	193.78 (78)		$5D_{5/2}$	193.32 (16)	
	385.143 (9)			213.16 (3)			242.56 (1)			198.43 (57)	
	810.69 (31)			493.13 (87)	482.642 [40]		593.0 (2.0)	585.677 [40]		225.63 (1)	
										234.773 (3)	
										459.57 (57)	509.687 [40]
$4S_{1/2}$	279.1332 (4)		$5S_{1/2}$	287.179 (7)		$6S_{1/2}$	334.71 (71)		$7S_{1/2}$	347.63 (5)	
	293.2134 (2)			299.64 (64)			362.58 (2)			363.36 (64)	
	361.524 (2)			309.13 (5)			378.373 (3)			394.63 (6)	
	361.691 (1)			309.303 (9)			421.40 (5)			466.94 (13)	
				371.754 (9)			474.62 (1)			518.78 (2)	
				447.386 (5)			477.559 (5)			526.778 (6)	
				448.088 (2)			1230.15 (6)			1381.01 (23)	
				1191.59 (1)							
$4D_{3/2}$	554.11 (12)		$4D_{3/2}$	317.850 (5)		$5D_{3/2}$	407.4377 (3)		$6D_{3/2}$	544.38 (62)	
	592.70 (3)			334.65 (1)			434.69 (23)			1316.93 (93)	
	1331.53 (53)			371.2822 (5)			481.52 (2)				
				375.78 (3)			573.80 (56)				
				471.96 (6)			649.82 (2)				
$4D_{5/2}$	507.25 (1)		$4D_{5/2}$	376.05 (3)		$5D_{5/2}$	436.25 (22)		$6D_{5/2}$	547.53 (53)	
	553.95 (95)			472.38 (6)			455.827 (4)			889.04 (23)	
	592.55 (3)			566.15 (10)			577.18 (57)			1287.17 (83)	
	811.9701 (4)						647.60 (2)				
	1329.45 (55)						1312.6247 (1)				

5. Conclusions

We identified a number of reliable magnetic-sublevel-independent tune-out wavelengths of many $S_{1/2}$ and $D_{3/2,5/2}$ states, and magic wavelengths of different combinations of $S_{1/2} - D_{3/2,5/2}$ transitions in the alkaline-earth ions from Mg^+ through Ba^+. If they can be measured precisely, accurate values of many electric dipole matrix elements can be inferred by combining the experimental values of these quantities with our theoretical results. Most of the magic wavelengths found from this study show that they can be detected using the red- and blue-detuned traps. In fact, it is possible to perform many high-precision measurements by trapping the atoms at the reported tune-out and magic wavelengths of the considered transitions in the future, which can be applied to different metrological studies.

Author Contributions: B.A. conceived the idea of magnetic-sublevel-independent magic and tune-out wavelengths for alkaline-earth ions which motivated J. to carry out this study. J. identified magic and tune-out wavelengths for the considered transitions in alkaline-earth ions and drafted the manuscript. H.K. verified the results and contributed in the editing of the manuscript. B.K.S. provided critical feedback and helped shape the research, analysis and manuscript. He also aided in interpretation and discussion of the results and commented on the manuscript. With the help of B.A., H.K. and B.K.S., J. modified this manuscript to the final version. All authors have read and agreed to the published version of the manuscript.

Funding: The work of B.A. is supported by SERB-TARE (TAR/2020/000189), New Delhi, India.

Institutional Review Board Statement: Not Applicable.

Informed Consent Statement: Not Applicable.

Data Availability Statement: The data underlying this article are available in the article.

Acknowledgments: Special thanks to the support of SERB-TARE (TAR/2020/000189), New Delhi, India.The employed relativistic many-body method was developed in the group of Professor M. S. Safronova of the University of Delaware, USA.

Conflicts of Interest: The authors declare no conflict of interest.

References

1. Hall, J.L.; Zhu, M.; Buch, P. Prospects for using laser-prepared atomic fountains for optical frequency standards applications. *JOSA B* **1989**, *6*, 2194–2205. [CrossRef]
2. Kostelecký, V.A.; Vargas, A.J. Lorentz and C P T tests with clock-comparison experiments. *Phys. Rev. D* **2018**, *98*, 036003. [CrossRef]
3. Wood, C.; Bennett, S.; Cho, D.; Masterson, B.; Roberts, J.; Tanner, C.; Wieman, C. Measurement of parity nonconservation and an anapole moment in cesium. *Science* **1997**, *275*, 1759–1763. [CrossRef]
4. Tiecke, T.; Thompson, J.D.; de Leon, N.P.; Liu, L.; Vuletić, V.; Lukin, M.D. Nanophotonic quantum phase switch with a single atom. *Nature* **2014**, *508*, 241–244. [CrossRef]
5. Xiaxing, X.; Mouqi, H.; Youyuan, Z.; Zhiming, Z. The parity non-conservation E1 matrix of barium-a semi-empirical calculation. *J. Phys. B Mol. Opt. Phys.* **1990**, *23*, 4239. [CrossRef]
6. Berengut, J.C.; Dzuba, V.A.; Flambaum, V.V. Isotope-shift calculations for atoms with one valence electron. *Phys. Rev. A* **2003**, *68*, 022502. [CrossRef]
7. Fortier, T.M.; Ashby, N.; Bergquist, J.C.; Delaney, M.J.; Diddams, S.A.; Heavner, T.P.; Hollberg, L.; Itano, W.M.; Jefferts, S.R.; Kim, K.; et al. Precision Atomic Spectroscopy for Improved Limits on Variation of the Fine Structure Constant and Local Position Invariance. *Phys. Rev. Lett.* **2007**, *98*, 070801. [CrossRef]
8. Roos, C.F.; Riebe, M.; Haffner, H.; Hansel, W.; Benhelm, J.; Lancaster, G.P.; Becher, C.; Schmidt-Kaler, F.; Blatt, R. Control and measurement of three-qubit entangled states. *Science* **2004**, *304*, 1478–1480. [CrossRef]
9. Kajita, M.; Li, Y.; Matsubara, K.; Hayasaka, K.; Hosokawa, M. Prospect of optical frequency standard based on a $^{43}Ca^+$ ion. *Phys. Rev. A* **2005**, *72*, 043404. [CrossRef]
10. Enderlein, M.; Huber, T.; Schneider, C.; Schaetz, T. Single ions trapped in a one-dimensional optical lattice. *Phys. Rev. Lett.* **2012**, *109*, 233004. [CrossRef]
11. Chou, C.w.; Hume, D.; Koelemeij, J.; Wineland, D.J.; Rosenband, T. Frequency comparison of two high-accuracy Al+ optical clocks. *Phys. Rev. Lett.* **2010**, *104*, 070802. [CrossRef] [PubMed]
12. Champenois, C.; Marciante, M.; Pedregosa-Gutierrez, J.; Houssin, M.; Knoop, M.; Kajita, M. Ion ring in a linear multipole trap for optical frequency metrology. *Phys. Rev. A* **2010**, *81*, 043410. [CrossRef]

13. Katori, H.; Ido, T.; Kuwata-Gonokami, M. Optimal design of dipole potentials for efficient loading of Sr atoms. *J. Phys. Soc. Jpn.* **1999**, *68*, 2479–2482. [CrossRef]
14. Liu, P.L.; Huang, Y.; Bian, W.; Shao, H.; Guan, H.; Tang, Y.B.; Li, C.B.; Mitroy, J.; Gao, K.L. Measurement of Magic Wavelengths for the $^{40}Ca^{+}$ Clock Transition. *Phys. Rev. Lett.* **2015**, *114*, 223001. [CrossRef]
15. Huang, Y.; Guan, H.; Li, C.; Zhang, H.; Zhang, B.; Wang, M.; Tang, L.; Shi, T.; Gao, K. Measurement of infrared magic wavelength for an all-optical trapping $^{40}Ca^{+}$ ion clock. *arXiv* **2022**, arXiv:2202.07828.
16. Kaur, J.; Singh, S.; Arora, B.; Sahoo, B. Magic wavelengths in the alkaline-earth-metal ions. *Phys. Rev. A* **2015**, *92*. [CrossRef]
17. Schneider, C.; Enderlein, M.; Huber, T.; Schätz, T. Optical trapping of an ion. *Nat. Photonics* **2010**, *4*, 772–775. [CrossRef]
18. Sackett, C.; Kielpinski, D.; King, B.; Langer, C.; Meyer, V.; Myatt, C.; Rowe, M.; Turchette, Q.; Itano, W.; Wineland, D.; et al. Experimental entanglement of four particles. *Nature* **2000**, *404*, 256–259. [CrossRef]
19. Tang, Y.B.; Qiao, H.X.; Shi, T.y.; Mitroy, J. Dynamic polarizabilities for the low lying states of Ca+. *Phys. Rev. A* **2013**, *87*, 042517. [CrossRef]
20. Ruffoni, M.; Den Hartog, E.; Lawler, J.; Brewer, N.; Lind, K.; Nave, G.; Pickering, J. Fe I oscillator strengths for the Gaia-ESO survey. *Mon. Not. R. Astron. Soc.* **2014**, *441*, 3127–3136. [CrossRef]
21. Wittkowski, M. Fundamental stellar parameters Technology roadmap for future interferometric facilities. In *Bulletin de la Sociètè Royale des Sciences de Liège, Proceedings of the European Interferometry Initiative Workshop Organized in the Context of the 2005 Joint European and National Astronomy Meeting "Distant Worlds", Liège, Belgium, 6–8 July 2005;* Surdej, J., Caro, D., Detal, A. , Eds.; Liège University, Institute of Astrophysics: Liège, Belgium, 2005; Volume 74, pp. 165–181.
22. LeBlanc, L.; Thywissen, J. Species-specific optical lattices. *Phys. Rev. A* **2007**, *75*, 053612. [CrossRef]
23. Catani, J.; Barontini, G.; Lamporesi, G.; Rabatti, F.; Thalhammer, G.; Minardi, F.; Stringari, S.; Inguscio, M. Entropy Exchange in a Mixture of Ultracold Atoms. *Phys. Rev. Lett.* **2009**, *103*, 140401. [CrossRef] [PubMed]
24. Wang, Y.; Zhang, X.; Corcovilos, T.A.; Kumar, A.; Weiss, D.S. Coherent Addressing of Individual Neutral Atoms in a 3D Optical Lattice. *Phys. Rev. Lett.* **2015**, *115*, 043003. [CrossRef] [PubMed]
25. Kotochigova, S.; Tiesinga, E. Controlling polar molecules in optical lattices. *Phys. Rev. A* **2006**, *73*, 041405. [CrossRef]
26. Rubio-Abadal, A.; Choi, J.y.; Zeiher, J.; Hollerith, S.; Rui, J.; Bloch, I.; Gross, C. Many-Body Delocalization in the Presence of a Quantum Bath. *Phys. Rev. X* **2019**, *9*, 041014. [CrossRef]
27. Holmgren, W.F.; Trubko, R.; Hromada, I.; Cronin, A.D. Measurement of a Wavelength of Light for Which the Energy Shift for an Atom Vanishes. *Phys. Rev. Lett.* **2012**, *109*, 243004. [CrossRef]
28. Herold, C.D.; Vaidya, V.D.; Li, X.; Rolston, S.L.; Porto, J.V.; Safronova, M.S. Precision Measurement of Transition Matrix Elements via Light Shift Cancellation. *Phys. Rev. Lett.* **2012**, *109*, 243003. [CrossRef]
29. Petrov, A.; Makrides, C.; Kotochigova, S. External field control of spin-dependent rotational decoherence of ultracold polar molecules. *Mol. Phys.* **2013**, *111*, 1731–1737. [CrossRef]
30. Henson, B.M.; Khakimov, R.I.; Dall, R.G.; Baldwin, K.G.H.; Tang, L.Y.; Truscott, A.G. Precision Measurement for Metastable Helium Atoms of the 413 nm Tune-Out Wavelength at Which the Atomic Polarizability Vanishes. *Phys. Rev. Lett.* **2015**, *115*, 043004. [CrossRef]
31. Kao, W.; Tang, Y.; Burdick, N.Q.; Lev, B.L. Anisotropic dependence of tune-out wavelength near Dy 741-nm transition. *Opt. Express* **2017**, *25*, 3411–3419. [CrossRef]
32. Heinz, A.; Park, A.J.; Šantić, N.; Trautmann, J.; Porsev, S.G.; Safronova, M.S.; Bloch, I.; Blatt, S. State-Dependent Optical Lattices for the Strontium Optical Qubit. *Phys. Rev. Lett.* **2020**, *124*, 203201. [CrossRef] [PubMed]
33. Arora, B.; Safronova, M.; Clark, C.W. Tune-out wavelengths of alkali-metal atoms and their applications. *Phys. Rev. A* **2011**, *84*, 043401. [CrossRef]
34. Bause, R.; Li, M.; Schindewolf, A.; Chen, X.Y.; Duda, M.; Kotochigova, S.; Bloch, I.; Luo, X.Y. Tune-Out and Magic Wavelengths for Ground-State $^{23}Na^{40}K$ Molecules. *Phys. Rev. Lett.* **2020**, *125*, 023201. [CrossRef] [PubMed]
35. Jiang, J.; Jiang, L.; Wang, X.; Zhang, D.H.; Xie, L.Y.; Dong, C.Z. Magic wavelengths of the Ca^{+} ion for circularly polarized light. *Phys. Rev. A* **2017**, *96*, 042503. [CrossRef]
36. Jiang, J.; Jiang, L.; Wang, X.; Shaw, P.; Zhang, D.H.; Xie, L.Y.; Dong, C.Z. Magic wavelengths of Ca^{+} ion for linearly and circularly polarized light. *J. Physics Conf. Ser.* **2017**, *875*, 122003. [CrossRef]
37. Chanu, S.R.; Koh, V.P.W.; Arnold, K.J.; Kaewuam, R.; Tan, T.R.; Zhang, Z.; Safronova, M.S.; Barrett, M.D. Magic wavelength of the Ba+138 6s S1/22–5d D5/22 clock transition. *Phys. Rev. A* **2020**, *101*, 042507. [CrossRef]
38. Jiang, J.; Ma, Y.; Wang, X.; Dong, C.Z.; Wu, Z. Tune-out and magic wavelengths of Ba^{+} ions. *Phys. Rev. A* **2021**, *103*, 032803. [CrossRef]
39. Singh, S.; Sahoo, B.; Arora, B. Magnetic-sublevel-independent magic wavelengths: Application to Rb and Cs atoms. *Phys. Rev. A* **2016**, *93*, 063422. [CrossRef]
40. Kaur, J.; Singh, S.; Arora, B.; Sahoo, B. Annexing magic and tune-out wavelengths to the clock transitions of the alkaline-earth-metal ions. *Phys. Rev. A* **2017**, *95*, 042501. [CrossRef]
41. Sherman, J.A.; Koerber, T.W.; Markhotok, A.; Nagourney, W.; Fortson, E.N. Precision Measurement of Light Shifts in a Single Trapped Ba^{+} Ion. *Phys. Rev. Lett.* **2005**, *94*, 243001. [CrossRef]
42. Sahoo, B.K.; Wansbeek, L.W.; Jungmann, K.; Timmermans, R.G.E. Light shifts and electric dipole matrix elements in Ba^{+} and Ra^{+}. *Phys. Rev. A* **2009**, *79*, 052512. [CrossRef]

43. Beloy, K. *Theory of the Ac Stark Effect on the Atomic Hyperfine Structure and Applications to Microwave Atomic Clocks*; University of Nevada: Reno, NV, USA, 2009.
44. Blundell, S.; Johnson, W.; Sapirstein, J. Relativistic all-order calculations of energies and matrix elements in cesium. *Phys. Rev. A* **1991**, *43*, 3407. [CrossRef] [PubMed]
45. Safronova, M.; Johnson, W. All-order methods for relativistic atomic structure calculations. *Adv. At. Mol. Opt. Phys.* **2008**, *55*, 191–233.
46. Sahoo, B.; Nandy, D.; Das, B.; Sakemi, Y. Correlation trends in the hyperfine structures of Fr 210, 212. *Phys. Rev. A* **2015**, *91*, 042507. [CrossRef]
47. Sahoo, B.; Das, B. Theoretical studies of the long lifetimes of the 6 d D 3/2, 5/2 2 states in Fr: Implications for parity-nonconservation measurements. *Phys. Rev. A* **2015**, *92*, 052511. [CrossRef]
48. Safronova, M.; Johnson, W.; Derevianko, A. Relativistic many-body calculations of energy levels, hyperfine constants, electric-dipole matrix elements, and static polarizabilities for alkali-metal atoms. *Phys. Rev. A* **1999**, *60*, 4476. [CrossRef]
49. Iskrenova-Tchoukova, E.; Safronova, M.S.; Safronova, U. High-precision study of Cs polarizabilities. *J. Comput. Methods Sci. Eng.* **2007**, *7*, 521–540. [CrossRef]
50. Safronova, U.; Johnson, W.; Safronova, M. Excitation energies, polarizabilities, multipole transition rates, and lifetimes of ions along the francium isoelectronic sequence. *Phys. Rev. A* **2007**, *76*, 042504. [CrossRef]
51. Kaur, M.; Dar, D.F.; Sahoo, B.; Arora, B. Radiative transition properties of singly charged magnesium, calcium, strontium and barium ions. *At. Data Nucl. Data Tables* **2020**, *137*, 101381. [CrossRef]
52. Arora, B.; Safronova, M.; Clark, C. Magic wavelengths for the np-ns transitions in alkali-metal atoms. *Phys. Rev. A* **2007**, *76*, 052509. [CrossRef]
53. Ralchenko, Y. NIST atomic spectra database. *Mem. Della Soc. Astron. Ital. Suppl.* **2005**, *8*, 96.
54. Barakhshan, P.; Marrs, A.; Bhosale, A.; Arora, B.; Eigenmann, R.; Safronova, M.S. *Portal for High-Precision Atomic Data and Computation*; (Version 2.0); University of Delaware: Newark, DE, USA. Available online: https://www.udel.edu/atom (accessed on 27 March 2022).
55. Kaur, M.; Singh, S.; Sahoo, B.; Arora, B. Tune-out and magic wavelengths, and electric quadrupole transition properties of the singly charged alkaline-earth metal ions. *At. Data Nucl. Data Tables* **2021**, *140*, 101422. [CrossRef]